RESEARCH PAPER

Glycosaminoglycans Modified Anionic Polysaccharide Nanoparticles For Enhancement of Antitumor Potential Via Inhibition of PI3K/AKT/mTOR Signaling Pathway

Reetesh Chourasia, Lokendra Singh Rathore, Rajesh Mujariya*
Institute of Pharmaceutical Science and Research, Sardar Patel University, Balaghat, M.P. India, 481001

Corresponding Author*
Rajesh Mujariya*
Institute of Pharmaceutical Science and Research, Sardar Patel University, Balaghat, M.P. India, 481001

Abstract
The present study focuses on the development of glycosaminoglycan-modified anionic polysaccharide nanoparticles (HG NPs) for enhancing the antitumor potential of 5-Fluorouracil (5-FU) through targeted inhibition of the PI3K/Akt/mTOR signaling pathway. Preformulation studies confirmed the suitability of 5-FU for nanoparticle formulation, exhibiting good solubility in organic solvents, a melting point of 282°C, and a characteristic λmax at 260 nm, ensuring reliable analytical quantification. FTIR and ^{1}H-NMR studies validated the successful incorporation of hyaluronic acid (HA), adipic dihydrazide (ADH), and gellan gum (GG) into the HG copolymer structure. Morphological evaluation using AFM revealed uniform spherical nanoparticles in the size range of 81–206 nm, while zeta potential analysis (-12.9 mV) confirmed good stability. Drug-loaded HG nanoparticles exhibited sustained and controlled drug release (97.87% over 48 h), significantly slower than GG nanoparticles. Hemolysis studies demonstrated reduced toxicity (4.27%) compared to free drug, indicating improved biocompatibility. In vitro cytotoxicity studies using A549 lung cancer cells showed enhanced efficacy of HG NPs with a lower IC_{50} (9.98 µg/mL) compared to free 5-FU. Flow cytometry studies revealed significant downregulation of mTOR expression and upregulation of p53, indicating effective modulation of cancer signaling pathways. Apoptosis analysis confirmed increased late apoptotic cell populations in HG NP-treated groups compared to free drug and GG nanoparticles. Overall, the developed HG nanoparticles demonstrated superior drug delivery, enhanced cytotoxicity, controlled release, and effective targeting of tumor signaling pathways, making them a promising system for cancer therapy.

Keywords: Glycosaminoglycans, Nanoparticles, 5-Fluorouracil, PI3K/Akt/mTOR Pathway, Antitumor Activity, Controlled Drug Delivery

How to cite this article: Chourasia R, Rathore LS, Mujariya R. Glycosaminoglycans modified anionic polysaccharide nanoparticles for enhancement of antitumor potential via inhibition of PI3K/AKT/mTOR signaling pathway. Int J Drug Deliv Technol. 2026;16(75s): 1648-1662. DOI: 10.25258/ijddt.16.75s.176

INTRODUCTION

Cancer is one of the leading causes of morbidity and mortality worldwide and continues to represent a major public health burden despite remarkable advances in diagnosis and treatment. It is characterized by uncontrolled cell proliferation resulting from genetic and epigenetic alterations that disrupt normal cellular regulatory mechanisms. These alterations enable cancer cells to evade apoptosis, sustain proliferative signaling, induce angiogenesis, invade surrounding tissues, and metastasize to distant organs. The increasing prevalence of cancer has created an urgent need for the development of novel therapeutic strategies capable of improving treatment efficacy while minimizing systemic toxicity. Conventional therapeutic approaches such as chemotherapy, radiotherapy, surgery, immunotherapy, and targeted therapy have significantly improved patient survival; however, treatment failure due to multidrug resistance, poor tumor selectivity, and severe adverse effects remains a major clinical challenge. Consequently, nanotechnology-based drug delivery systems have emerged as promising alternatives for enhancing the therapeutic index of anticancer agents by enabling targeted drug delivery and controlled drug release (Deng et al., 2024).

Among all malignancies, lung cancer remains the most frequently diagnosed cancer and the leading cause of cancer-related deaths worldwide. Lung cancer is broadly classified into non-small cell lung cancer (NSCLC), accounting for approximately 85% of cases, and small cell lung cancer (SCLC), representing the remaining 15%. NSCLC includes adenocarcinoma, squamous cell carcinoma, and large-cell carcinoma. The high mortality associated with lung cancer is primarily attributed to delayed diagnosis, rapid metastatic progression, genetic heterogeneity, and the development of resistance to conventional chemotherapy and targeted therapies. Despite improvements in screening techniques and

the introduction of immune checkpoint inhibitors and molecular targeted drugs, the overall five-year survival rate for advanced lung cancer remains unsatisfactory. Therefore, innovative therapeutic approaches capable of specifically targeting tumor tissues while reducing systemic toxicity are urgently required (Qiang et al., 2025).

According to recent global cancer statistics, lung cancer accounts for approximately 2.48 million new cases annually, representing 12.4% of all newly diagnosed cancers, and is responsible for nearly 1.8 million cancer-related deaths, accounting for 18.7% of total cancer mortality worldwide. These alarming statistics highlight the enormous global health burden posed by lung cancer and emphasize the necessity for more effective therapeutic interventions. Tobacco smoking remains the principal risk factor; however, environmental pollution, occupational carcinogens, genetic susceptibility, and lifestyle-related factors also contribute significantly to disease incidence. The increasing prevalence of lung cancer, particularly in developing countries, underscores the importance of developing advanced drug delivery systems capable of improving treatment outcomes (Pang et al., 2026).

Cancer progression is regulated by multiple intracellular signaling pathways that coordinate cell growth, proliferation, metabolism, apoptosis, and survival. Among these, the phosphatidylinositol-3-kinase/protein kinase B/mammalian target of rapamycin (PI3K/AKT/mTOR) signaling pathway is one of the most extensively investigated oncogenic pathways. Under physiological conditions, this signaling cascade regulates normal cellular functions, including protein synthesis, glucose metabolism, cell cycle progression, and survival. However, genetic mutations, receptor tyrosine kinase activation, phosphatase and tensin homolog (PTEN) loss, and amplification of PI3K frequently lead to constitutive activation of the pathway in numerous human cancers, including lung cancer. Persistent activation of the PI3K/AKT/mTOR pathway promotes uncontrolled proliferation, inhibits apoptosis, enhances angiogenesis, facilitates epithelial–mesenchymal transition, and contributes to drug resistance, thereby accelerating tumor progression. Consequently, inhibition of this pathway has emerged as a promising therapeutic strategy for improving anticancer efficacy (Qiang et al., 2025).

Recent advances in molecular oncology have demonstrated that pharmacological inhibition of PI3K, AKT, or mTOR significantly suppresses tumor growth and enhances the sensitivity of cancer cells to chemotherapeutic agents. Nevertheless, the clinical application of many pathway inhibitors remains limited due to poor aqueous solubility, rapid degradation, nonspecific biodistribution, dose-limiting toxicity, and inadequate accumulation within tumor tissues. These limitations have stimulated growing interest in nanotechnology-based drug delivery systems that can improve the pharmacokinetic properties of anticancer drugs and selectively deliver therapeutic agents to tumor cells. Nanoparticle-mediated drug delivery enhances drug stability, prolongs circulation time, improves cellular uptake, and reduces systemic toxicity while maximizing therapeutic efficacy through passive and active targeting mechanisms.

Nanotechnology has emerged as one of the most promising approaches in modern cancer therapy owing to its ability to improve the pharmacokinetic and pharmacodynamic properties of anticancer drugs. Nanoparticles are colloidal carriers ranging from 1 to 1000 nm in size that can encapsulate therapeutic agents, protect them from premature degradation, and facilitate controlled as well as site-specific drug release. Compared with conventional formulations, nanoparticle-based drug delivery systems offer several advantages, including enhanced drug solubility, prolonged circulation time, improved bioavailability, reduced systemic toxicity, and increased therapeutic efficacy. Furthermore, nanoparticles preferentially accumulate within tumor tissues through the enhanced permeability and retention (EPR) effect, resulting from the leaky vasculature and impaired lymphatic drainage characteristic of solid tumors. Surface modification of nanoparticles with targeting ligands further improves selective uptake by cancer cells, thereby minimizing off-target effects and enhancing therapeutic outcomes (Mitragotri et al., 2021; Shi et al., 2020).

Among various nanocarriers, natural polysaccharide-based nanoparticles have gained considerable attention because of their excellent biocompatibility, biodegradability, low immunogenicity, and ease of chemical modification. Polysaccharides such as chitosan, alginate, dextran, pectin, gellan gum, and glycosaminoglycans provide versatile platforms for the development of targeted drug delivery systems. Their abundant functional groups permit conjugation with drugs, targeting ligands, imaging probes, and stimuli-responsive moieties, enabling the design of multifunctional nanomedicines. Additionally, these polymers exhibit favorable physicochemical properties that improve drug loading efficiency, sustained drug release, and stability under physiological conditions, making them attractive candidates for cancer therapy (Liu et al., 2022).

Glycosaminoglycans (GAGs) are naturally occurring linear anionic polysaccharides present in the extracellular matrix and connective tissues. They include hyaluronic acid, chondroitin sulfate, heparin, heparan sulfate, dermatan sulfate, and keratan sulfate. These biomacromolecules regulate

numerous biological processes, including cell proliferation, migration, differentiation, inflammation, angiogenesis, and tissue repair. Due to their excellent biocompatibility and intrinsic biological activity, glycosaminoglycans have emerged as promising materials for biomedical applications, particularly in targeted drug delivery and regenerative medicine. Chemical modification of glycosaminoglycans allows the fabrication of nanoparticles with enhanced stability, controlled drug release characteristics, and improved tumor-targeting capabilities. Consequently, glycosaminoglycan-modified nanoparticles have attracted increasing attention as advanced nanocarriers for cancer diagnosis and therapy (Volpi et al., 2021).

Among all glycosaminoglycans, hyaluronic acid (HA) is one of the most extensively investigated polymers for targeted cancer therapy. HA is a naturally occurring, non-sulfated anionic polysaccharide composed of repeating units of D-glucuronic acid and N-acetyl-D-glucosamine linked through β-(1→3) and β-(1→4) glycosidic bonds. It is widely distributed throughout connective tissues, synovial fluid, vitreous humor, and the extracellular matrix. Owing to its exceptional biocompatibility, biodegradability, non-toxicity, and hydrophilicity, HA has been widely employed as a drug carrier in nanomedicine. More importantly, HA exhibits a strong affinity for the CD44 receptor, which is highly overexpressed in numerous malignancies, including lung, breast, ovarian, colorectal, pancreatic, and gastric cancers. This receptor-mediated interaction enables HA-functionalized nanoparticles to selectively bind to tumor cells and undergo receptor-mediated endocytosis, thereby significantly improving intracellular drug delivery and reducing systemic toxicity (Misra et al., 2015; Huang & Huang, 2018).

The ability of hyaluronic acid nanoparticles to actively target CD44-positive cancer cells has made them highly effective carriers for chemotherapeutic drugs, nucleic acids, proteins, and small-molecule inhibitors. Following receptor-mediated internalization, HA nanoparticles enhance intracellular drug accumulation and improve therapeutic efficacy by overcoming multidrug resistance mechanisms. In addition to serving as targeting ligands, HA-based nanocarriers improve circulation time, increase tumor retention, reduce immune recognition, and enhance drug stability. These multifunctional characteristics make HA one of the most promising biomaterials for precision cancer therapy. Recent investigations have also demonstrated that HA-coated nanoparticles can effectively deliver inhibitors of oncogenic signaling pathways, including the PI3K/AKT/mTOR pathway, resulting in suppression of tumor proliferation, induction of apoptosis, inhibition of angiogenesis, and reduction of metastatic progression (Zhang et al., 2023).

Gellan gum (GG) is another naturally derived anionic polysaccharide produced by *Sphingomonas elodea*. It possesses excellent gel-forming ability, biocompatibility, biodegradability, mechanical strength, and mucoadhesive properties, making it an attractive biomaterial for pharmaceutical and biomedical applications. Gellan gum nanoparticles exhibit high drug encapsulation efficiency, sustained drug release behavior, and remarkable physicochemical stability. Furthermore, the abundant carboxyl groups present in gellan gum facilitate ionic cross-linking and chemical conjugation with targeting molecules such as hyaluronic acid. These characteristics enable the fabrication of multifunctional hybrid nanoparticles with improved stability and enhanced targeting efficiency (Osmałek et al., 2014).

The combination of hyaluronic acid and gellan gum offers a highly promising strategy for developing advanced nanocarriers for targeted anticancer drug delivery. In such hybrid nanoparticle systems, gellan gum provides structural integrity, mechanical stability, and controlled drug release, whereas hyaluronic acid confers active tumor-targeting capability through CD44 receptor recognition. This synergistic combination enhances nanoparticle accumulation within tumor tissues while minimizing exposure to healthy organs, thereby improving therapeutic efficacy and reducing adverse effects. Furthermore, the sustained release characteristics of gellan gum maintain therapeutic drug concentrations over prolonged periods, while HA-mediated receptor targeting significantly increases intracellular drug uptake by cancer cells. These combined advantages contribute to enhanced inhibition of tumor growth and metastasis (Liu et al., 2022).

Growing evidence indicates that nanoparticle-mediated delivery of anticancer agents can effectively modulate dysregulated intracellular signaling pathways associated with tumor progression. Among these, inhibition of the PI3K/AKT/mTOR signaling pathway has become a major focus because of its critical role in regulating cancer cell proliferation, metabolism, survival, angiogenesis, and therapeutic resistance. HA-modified gellan gum nanoparticles facilitate efficient intracellular delivery of anticancer drugs capable of suppressing this pathway, thereby inducing apoptosis, inhibiting cell cycle progression, reducing angiogenesis, and overcoming drug resistance. The integration of targeted delivery with molecular pathway inhibition represents an innovative therapeutic strategy for improving treatment outcomes in lung cancer and other solid malignancies (Fruman et al., 2017; Janku et al., 2018).

Conclusion

Overall, the integration of hyaluronic acid with gellan gum in nanoparticle formulations represents a promising strategy for improving anticancer therapy. The HA component provides targeted delivery through CD44 receptor recognition, while gellan gum offers structural stability and controlled drug release. Together, these properties enhance drug bioavailability, increase tumor-specific accumulation, and effectively inhibit critical oncogenic pathways such as PI3K/AKT/mTOR. Consequently, HA-modified gellan gum nanoparticles hold significant potential as an advanced nanomedicine platform for targeted cancer treatment and improved therapeutic outcomes.

Materials

5-Fluorouracil (5-FU) was obtained as a gift sample from Neon Pharmaceuticals (MS, India). GG (Gellan gum) (Mol. Wt. 6000 Daltons) was acquired from Central Drug House (CDH), Delhi, India. Hyaluronic Acid (HA) was charitably supplied by Himedia located in Mumbai, India. N-hydroxysuccinimide (NHS), dialysis membranes, 1-ethyl-3-(3- dimethylaminopropyl) carbodiimide hydrochloride (EDAC), Dicyclohexyl Carbodiimide (DCC), Pluronic F-68 were purchased from Himedia laboratories, Mumbai, India. Adipic acid dihydrazide (ADH) was purchased from Sigma Aldrich. Acetone, isopropyl alcohol and acetonitrile purchased from Merck Limited, Mumbai India and other chemicals which are consumed are of investigative chemical grade and used as brought.

Methodology

Synthesis of Hyaluronic Acid–ADH–Gellan Gum (HG) Copolymer

Hyaluronic acid–adipic acid dihydrazide–gellan gum (HA–ADH–GG; HG) copolymer was synthesized through carbodiimide-mediated coupling. Initially, 100 mg of hyaluronic acid (HA) was dissolved in 10 mL of distilled water under continuous stirring until a clear solution was obtained. The carboxyl groups of HA were activated by adding 500 mg of 1-ethyl-3-(3-dimethylaminopropyl) carbodiimide (EDAC), followed by the addition of 500 mg of adipic acid dihydrazide (ADH). The reaction mixture was stirred for 6 h at room temperature to obtain the HA–ADH conjugate.

Separately, 100 mg of gellan gum (GG) was dispersed in 10 mL of double-distilled water at 60°C with continuous stirring. The GG solution was activated by adding 100 mg of dicyclohexylcarbodiimide (DCC) and 50 mg of N-hydroxysuccinimide (NHS), and the reaction was maintained for 12 h to activate the carboxyl groups. The activated GG solution was then added dropwise to the HA–ADH solution under constant stirring and allowed to react for an additional 6 h. The coupling between the amino groups of ADH and activated carboxyl groups of GG resulted in the formation of stable amide bonds, producing the HA–ADH–GG (HG) copolymer. The synthesized copolymer was vacuum dried and characterized by Fourier Transform Infrared (FTIR) spectroscopy and ^{1}H Nuclear Magnetic Resonance (^{1}H-NMR) spectroscopy to confirm successful conjugation and amide bond formation.

Preparation of HG and GG Nanoparticles

Drug-loaded HG nanoparticles were prepared by the solvent diffusion technique. The synthesized HG copolymer (10–30 mg) was dissolved in 20 mL of acetone, and 5-fluorouracil (5-FU, 30 mg) dissolved in acetone was added dropwise under continuous stirring. Separately, Pluronic F-68 (250 mg) was dissolved in distilled water to prepare 1% and 2% stabilizer solutions. The drug–polymer solution was slowly introduced into the aqueous Pluronic solution under magnetic stirring for 6 h, resulting in nanoparticle formation through solvent diffusion and polymer precipitation.

The nanoparticle suspension was filtered through a 0.45 µm membrane filter and centrifuged at 12,000 rpm for 10 min. The collected nanoparticle pellet was freeze-dried (lyophilized) to obtain dry HG nanoparticles. Plain GG nanoparticles (without HA modification) were prepared using the same procedure for comparative evaluation.

The HA-functionalized HG nanoparticles are expected to enhance selective tumor targeting through CD44 receptor-mediated uptake, improve intracellular drug delivery, provide sustained drug release, and increase the therapeutic efficacy of encapsulated 5-fluorouracil compared with plain GG nanoparticles.

Characterization parameters

Surface Characteristics by Atomic Force Microscopy (AFM)

The surface morphology and structural characteristics of the prepared nanoparticles were analyzed using Atomic Force Microscopy (AFM) (SPM-9500, Shimadzu) operated in contact mode. The analysis was performed using a silicon micro-cantilever probe. A small amount of nanoparticle suspension containing plain Gellan gum (GG) nanoparticles and Hyaluronic acid (HA)-modified nanoparticles was deposited onto a freshly cleaved mica substrate. The sample was allowed to remain on the substrate for approximately one minute to ensure proper adsorption and then gently dried using a stream of air to remove excess solvent.

Particle Size and Zeta Potential Analysis

The average particle size, polydispersity index (PDI), and zeta potential of the formulated nanoparticles were determined using a Malvern

particle size analyzer (DTS Ver. 4.10, Malvern Instruments, UK) (Garg et al., 2016a).

Differential Scanning Calorimetry (DSC) Analysis

The thermal behavior and physicochemical state of the prepared nanoparticles were evaluated using Differential Scanning Calorimetry (DSC) with a DSC-60 instrument (Shimadzu, Kyoto, Japan). Approximately 10 mg of each sample including Hyaluronic acid (HA), Fluorouracil (5-FU), plain HG copolymer, and 5-FU-loaded HG nanoparticles were sealed in aluminum pans and subjected to thermal scanning (Garg et al., 2016a).

Entrapment Efficiency

The entrapment efficiency of 5-FU-loaded HA-modified nanoparticles (HG NPs) and plain GG nanoparticles was determined using High-Performance Liquid Chromatography (HPLC).

Approximately 10 mg of nanoparticle formulation was dispersed in acetone to extract the drug. The dispersion was centrifuged at 5000 rpm for 15 minutes using a cooling centrifuge to remove polymeric debris. The clear supernatant was collected and analyzed using an HPLC system at a detection wavelength of 260 nm to determine the amount of drug encapsulated within the nanoparticle system.

In-vitro Drug Release Study

The in-vitro release of Fluorouracil (5-FU) from HA-modified nanoparticles and GG nanoparticles was studied using the dialysis membrane diffusion method. The drug-loaded nanoparticle formulations were separately placed inside dialysis bags (HiMedia) and immersed in 50 mL of phosphate-buffered saline (PBS) solution at pH 7.4. The system was maintained at 37 ± 2°C with constant stirring at 100 rpm to simulate physiological conditions. At predetermined time intervals, 1 mL of release medium was withdrawn and replaced with an equal volume of fresh buffer solution to maintain sink conditions. The amount of drug released into the medium was quantified using the HPLC system (Waters HPLC, Model-515) (Garg et al., 2019; Weng et al., 2020).

Hemolytic Toxicity Study

The hemolytic activity of the developed nanoparticle formulations was evaluated to assess their compatibility with red blood cells (RBCs). Fresh human blood samples were collected in sterile collection tubes and centrifuged at 10,000 rpm for 10 minutes to separate RBCs from plasma. The plasma was discarded, and the RBC pellet was washed and resuspended in normal saline to obtain 10% hematocrit suspension. For the positive control, 1 mL of RBC suspension was mixed with 10 mL distilled water, which produces complete hemolysis (100% hemolysis standard). For test samples, the drug-loaded HA nanoparticles were incubated with the hematocrit suspension up to a final volume of 10 mL. The samples were incubated at 37°C for 1–2 hours, followed by centrifugation at 5000 rpm for 5 minutes. The absorbance of the supernatant was measured at 540 nm using a spectrophotometer to determine the percentage of hemolysis caused by the nanoparticle formulations (Garg et al., 2016b; Bhadra et al., 2005).

Sulforhodamine B (SRB) Cytotoxicity Assay

The cytotoxic activity of the developed nanoparticle formulations was evaluated using the Sulforhodamine B (SRB) assay, a sensitive and reliable method based on the measurement of cellular protein content. Human lung cancer A549 cells were cultured in suitable growth medium at 37°C in a humidified atmosphere containing 5% CO_2. Approximately 1×10^4 cells/well were seeded into 96-well plates and incubated for 24 h to allow cell attachment. The cells were then treated with HA-modified nanoparticle formulations at concentrations of 10, 20, 40, and 80 µg/mL and further incubated for 48 h. Following treatment, the cells were fixed with 10% trichloroacetic acid (TCA), stained with 0.4% SRB solution, and washed with 1% acetic acid to remove unbound dye. The protein-bound dye was dissolved in Tris buffer, and the absorbance was measured at 540 nm using an ELISA reader. The reduction in absorbance compared with untreated control cells was used to determine the cytotoxic activity of the nanoparticle formulations (Garg et al., 2019).

mTOR Assay

The monoclonal antibody O21-404 specifically recognizes the human mammalian target of rapamycin phosphorylated at serine residue 2448, commonly referred to as mTOR (pS2448). mTOR signaling pathway plays a crucial role in regulating cellular growth, metabolism, and survival.

Human lung cancer A549 cells were seeded in 6-well plates at a density of 3×10^5 cells/well and incubated at 37°C in 5% CO_2 for 24 h. The cells were then treated with 5-FU-loaded HA-modified nanoparticles and corresponding control formulations for an additional 24 h. After treatment, the cells were washed with PBS, detached using Trypsin-EDTA, collected by centrifugation (300 × g, 5 min), and washed twice with PBS. The cell pellets were fixed in 70% chilled ethanol for 30 min, washed to remove residual ethanol, and incubated with 5 µL of mTOR-PE conjugated antibody for 30 min in the dark at room temperature. After washing with PBS containing 0.1% sodium azide, the cells were resuspended in 0.5 mL PBS and analyzed by flow cytometry to determine the expression level of

phosphorylated mTOR (pS2448) following treatment with the nanoparticle formulations.

p53 expression

p53 tumor suppressor protein is a 53 kDa nuclear phosphoprotein that functions as a critical tumor suppressor involved in regulating the cellular response to DNA damage. Upon genomic stress, p53 activates transcription of several genes responsible for cell cycle arrest, DNA repair, and apoptosis, thereby preventing the propagation of damaged cells. The p53 gene is the most frequently mutated gene identified in human cancers, including tumors of the colon, lung, breast, ovary, and bladder. In many cancer cells, missense mutations lead to the accumulation and overexpression of mutant p53 proteins. Wild-type p53 normally exhibits a short half-life and is often undetectable in normal tissues.

Human lung cancer A549 cells were seeded in 6-well plates at a density of 3×10^5 cells/well and incubated at 37°C in 5% CO_2 for 24 h. The cells were then treated with 5-FU-loaded HA-modified nanoparticles and appropriate control formulations for 24 h. After treatment, the cells were washed with PBS, detached using Trypsin-EDTA, collected by centrifugation (300 × g, 5 min), and washed twice with PBS. The cell pellets were fixed with 70% chilled ethanol for 30 min, washed to remove residual ethanol, and incubated with 5 µL of p53-FITC conjugated antibody for 30 min in the dark at room temperature. Following washing with PBS containing 0.1% sodium azide, the cells were resuspended in 0.5 mL PBS and analyzed by flow cytometry to determine p53 protein expression after treatment with the nanoparticle formulations.

Apoptosis Assay

In this study, an apoptosis assay was performed on A549 lung cancer cells to assess the cytotoxicity of 5-FU, 5-FU-loaded HG NPs, and 5-FU-loaded GG NPs. The assay utilized Annexin V-FITC/PI staining in combination with flow cytometry to measure apoptosis induction. The A549 cells were treated with various concentrations of 5-FU, 5-FU-loaded HG NPs, and 5-FU-loaded GG NPs, and the percentage of apoptotic cells was evaluated. In this protocol, the cells were first treated with the nanoparticles or free drug for a specified period, after which they were stained with Annexin V-FITC and Propidium Iodide (PI), marking early apoptotic and late apoptotic cells, respectively. Flow cytometry analysis was used to quantify early apoptosis (Annexin V-positive/PI-negative) and late apoptosis/necrosis (Annexin V-positive/PI-positive), and viable cells (Annexin V-negative/PI-negative). This method allows for the precise determination of apoptosis levels induced by each treatment (Garg et al., 2019).

Statistical analysis

Final research outcomes were shown as mean ± SD. This evaluation was achieved by t-test . $P < 0.05$ was also important. All processes were performed thrice.

3. Results & Discussion

^{1}H-NMR and FTIR spectroscopic analysis

The 1H-NMR and FTIR spectrometers were used to validate the HG copolymer. Figure 1 & 2, shows a spectroscopic graph of 1H-NMR and FTIR. The FTIR measurements yielded spectra ranging from 3600 cm^{-1} to 400 cm^{-1}. The FTIR spectrum of Hyaluronic Acid (HA) typically exhibits prominent absorption bands at specific wavenumbers, each corresponding to key functional groups within its molecular structure. The band at 3317 cm^{-1} is attributed to the O-H and N-H stretching vibrations, which are characteristic of the hydroxyl and amine groups present in HA. The absorption peak at 2850 cm^{-1} corresponds to C-H stretching vibrations, reflecting the presence of methylene (CH_2) and methyl (CH_3) groups. Another significant peak appears at 1645 cm^{-1}, corresponding to amide I, which includes C=O stretching, an important feature of the amide functional group. The 1565 cm^{-1} peak is assigned to amide II, which reflects bending vibrations from N-H. Finally, the peak at 1037 cm^{-1} corresponds to C-O-C stretching, confirming the polysaccharide structure of HA. Collectively, these FTIR peaks confirm the presence of both carboxyl and amide functional groups, which are essential features of HA's complex molecular structure. In the case of Gellan Gum (GG), the FTIR spectrum reveals several characteristic peaks that provide insight into its molecular makeup. The broad peak at 3250 cm^{-1} is indicative of O-H stretching vibrations from the hydroxyl groups, a hallmark of polysaccharides like GG. The 2930 cm^{-1} peak corresponds to C-H stretching vibrations, specifically from the CH_2 and CH_3 groups, present in the sugar units. At 1745 cm^{-1}, a C=O stretching vibration is observed, typically associated with ester or carboxyl groups, confirming the presence of these functional groups in GG. The peak at 1590 cm^{-1} reflects C=C stretching, which indicates the presence of the sugar backbone, particularly from galacturonic acid or glucose units. The final important peak at 1100 cm^{-1} corresponds to C-O stretching, a signature feature of the polysaccharide structure of GG. These peaks together confirm the polysaccharide nature of GG and the presence of various functional groups that contribute to its overall structure (Fig 1 a). Peaks observed at 3255 cm^{-1} due to amide N-H stretch, 2740 cm^{-1} and 1380 cm^{-1} due to the presence of C-H alkene bonds, 1750 cm^{-1} due to the presence of C=O stretch, 1640 cm^{-1} also showing C=O bond formation, 1285 cm^{-1} due to C-N stretching of the amide bond, and 1095

cm^{-1} due to C=O stretching were the peaks obtained by FTIR spectra. The existence of an amide bond as well as a C=O carboxyl bond is confirmed by the appearance of characteristic peaks at 3255 cm^{-1} and 1640 cm^{-1}, confirming the formation of an amide bond between the amine group of ADH and both carboxyl groups of Hyaluronic Acid (HA) and Gellan Gum (GG) (Fig 1b).

Fig. 1 (a). FTIR spectrum of HA and GG.

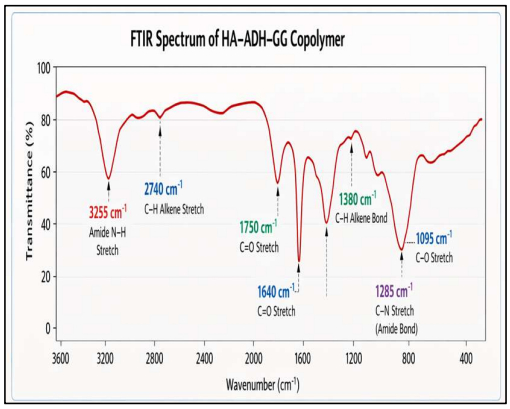

Figure 2 displays the ^{1}H-NMR spectra of the HG copolymer. The spectra reveal identical peaks that confirm the presence of Hyaluronic Acid (HA), Adipic Acid Dihydrazide (ADH), and Gellan Gum (GG) within the HG copolymer structure.

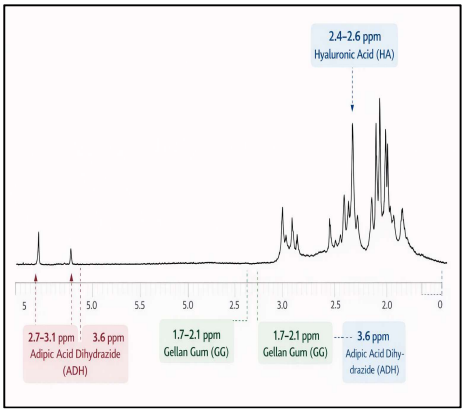

Fig. 1 (b). FTIR spectrum of HG copolymer

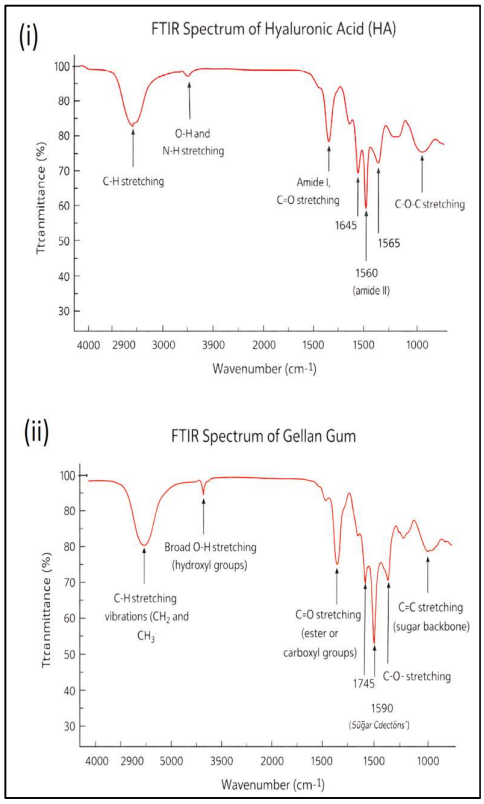

Fig. 2. NMR spectra of FG copolymer

The proton assignment of HA is observed in the range of 2.4-2.6 ppm, which corresponds to the protons in the glucuronic acid and acetyl groups present in the HA structure. These protons are typically part of the sugar backbone and its functional groups. The peak of GG appears between 1.7-2.1 ppm, indicating the presence of protons in the gellan gum structure. This region is attributed to the CH2 groups in the glucose and rhamnose units that make up GG, confirming the integration of GG into the copolymer. For Adipic Acid Dihydrazide (ADH), the proton assignments are observed at 2.7-3.1 ppm and 3.6 ppm. The signals at 2.7-3.1 ppm are characteristic of the -NH-CH2- groups of ADH, while the peak at 3.6 ppm corresponds to the NH2 group in the dihydrazide structure. The proton assignments for HA, ADH, and GG clearly demonstrate the incorporation of all three components in the HG copolymer. These assignments validate the successful conjugation of HA, ADH, and GG, and confirm the compatibility between HG and GG in the copolymer structure.

Surface Characteristics

A method called Atomic Force Microscopy (AFM) (SPM-9500, Shimadzu) was utilized to assess the surface properties of the Hyaluronic Acid (HA) nanoparticles, including their form, size, and texture. AFM is a powerful technique that provides

high-resolution nanoscale surface imaging, capable of producing both topographical and mechanical property maps of materials. The AFM setup used for the analysis was capable of both contact and non-contact imaging, providing insights into the surface roughness, morphology, and dimensional characteristics of the nanoparticles. As observed in AFM images (Figure 3), captured in both single- and 3D modes, the produced HA nanoparticles exhibited a uniform spherical morphology. The nanoparticles were consistently sized within the nanometric range, with diameters measured between 81-206 nm, confirming their nanoparticulate nature. The 3D AFM images clearly demonstrated the spherical shape of the nanoparticles, with no significant aggregation or structural irregularities.

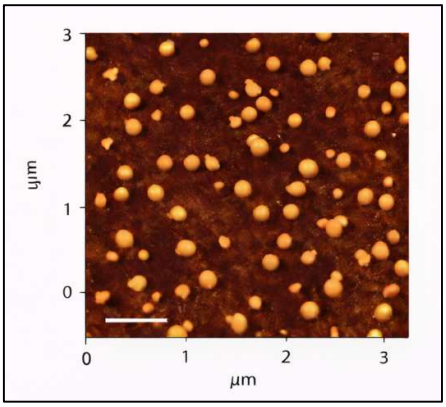

Figure 3 (a): AFM image of HG nanoparticles

In addition to size, the AFM analysis also revealed that the nanoparticles had identical heights across the sample. This uniformity was further corroborated by the height profile generated from the AFM topography scans, which showed consistent elevations across the surface, suggesting a well-defined and uniform nanostructure, which is often crucial for biocompatibility and drug delivery applications. The AFM data, including particle distribution and surface uniformity, were in excellent agreement with previous reports on HA nanoparticles, confirming their nanoscale uniformity and spherical morphology. These results suggest that the HA nanoparticles have desirable characteristics for potential applications in drug delivery, biomedical fields, and nanomedicine, where uniformity and controlled size are essential parameters for effectiveness and stability.

Atomic Force Microscopy (AFM) analysis of Gellan Gum (GG) nanoparticles revealed a particle size of 102 nm, which was slightly larger than the Hyaluronic Acid (HA) nanoparticles. The AFM images clearly showed that the GG nanoparticles were agglomerated, indicating that the particles tend to cluster together, forming aggregates. This agglomeration is likely a result of the polymeric nature of GG, which influences the interparticle interactions. The particle size observed in AFM images was consistent with the size distribution found in the particle size analyzer data, confirming the nanometric size range of GG nanoparticles. This agglomeration may have implications for the stability and drug delivery efficiency of GG nanoparticles, highlighting the need for potential optimization in formulation processes to reduce aggregation and enhance nanoparticle dispersion.

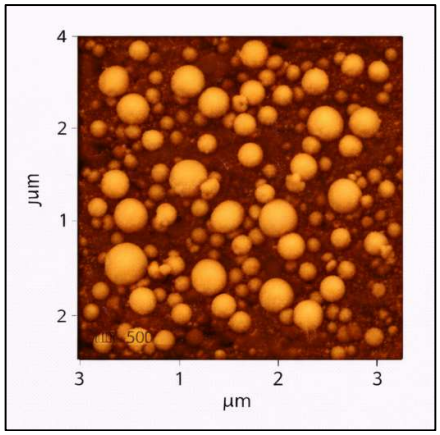

Figure 3 (b): AFM image of GG nanoparticles

Zeta Potential Determination, Particle Size analysis and Drug Entrapment Proficiency

A particle size analyzer was used to evaluate the particle size of HG nanoparticles. The particle size of HG nanoparticles was found to be 81.2±0.95 nm. Due to particle aggregation, the particle size distribution ranges from 81.2±0.95 nm to 206.9±1.50 nm. The size of particles increases from 81 nm to 206 nm when the quantity of Gellan Gum (GG) (GG-polymer) is increased from 10 mg to 30 mg, according to the results shown in Table 7.7. Similarly, the particle sizes derived from GG NPs ranged from 102.4±1.15 nm to 280.7±1.95 nm (Table 7.8). The polydispersity index (PDI) of HG nanoparticles was determined to be 0.062 ± 0.04, whereas GG nanoparticles had a PDI value of 0.068 ± 0.09. The encapsulation efficiency of the manufactured HG nanoparticles and GG nanoparticles was found to be 94.43±1.25% and 89.31±1.10%, respectively, while the zeta potential of HG was found to be -12.9 mV and -6.12 mV for GG NPs (Table 1 and Figure 4). The size of nanoparticles was altered by varying the concentrations of surfactant and polymers, according to the results shown in the table. When the amount of GG (polymer) is increased from 10 mg to 30 mg, the size of HG particles increases from 81 nm to 206 nm, and the entrapment efficiency (drug content) decreases from 94% to

71%. This suggests that as particle size increases, the efficiency of entrapment decreases (Table 1,2). GG nanoparticles, like HG NPs, were impacted by polymer concentration. Increasing the quantity of GG (polymer) from 10 mg to 30 mg increased the particle size from 102 nm to 280 nm. Because of the greater size of the particles and the higher quantity of polymer concentration, the entrapment efficiency of GG nanoparticles was found to decrease from 89% to 61% (Table 3).

Table 1. Ingredients and concentration using in the formulation of HG nanoparticles.

S. No.	Drug: Polymer ratio (mg)	Internal phase			External phase		% Entrapment efficiency	Particle size (nm)
		5-FU (mg)	HG (mg)	Acetone (ml)	Pluronic F-68 (mg)	Water (ml)		
S1	30:10	30	10	20	250	25	74.65 ±1.50	195.8±1.75
S2	30:20	30	20	20	250	25	81.56 ±1.15	141.7±1.50
S3	30:30	30	30	20	250	25	**94.43 ±1.25**	**81.2 ±0.95**
S4	30:10	30	10	20	500	25	71.37 ±0.50	206.9±1.50
S5	30:20	30	20	20	500	25	78.32 ±0.98	164.3±1.25
S6	30:30	30	30	20	500	25	86.98 ±0.50	115.4±1.10

S: Sample, 5-FU: 5-Fluorouracil

Table 2. Ingredients and concentration using in the formulation of GG nanoparticles.

S. No.	Drug: Polymer ratio (mg)	Internal phase			External phase		% Entrapment efficiency	Particle size (nm)
		5-FU (mg)	GG (mg)	Acetone (ml)	Pluronic F-68 (mg)	Water (ml)		
S1	30:10	30	10	20	250	25	64.18 ±1.95	253.8±2.25
S2	30:20	30	20	20	250	25	75.50 ±1.50	196.2±1.30
S3	30:30	30	30	20	250	25	**89.31 ±1.10**	**102.4±1.15**
S4	30:10	30	10	20	500	25	63.25 ±020	280.7±1.95
S5	30:20	30	20	20	500	25	69.15 ±1.70	232.7±2.15
S6	30:30	30	30	20	500	25	83.43 ±1.25	139.9±1.50

S: Sample, 5-FU: 5-Fluorouracil

Table 3. Optimum particle size &entrapment efficiency of HG and GG nanoparticles

S. No.	Formulations	Entrapment efficiency	Particle size (nm)	Polydispersity Index	Zeta Potential
1	HG NPs	94.43± 1.25	81.2± 0.95	0.062±0.04	-12.9 mV
2.	GG NPs	89.31± 1.10	102.4 ±1.15	0.068±0.09	-6.12 mV

The concentration of surfactant (Pluronic F-68) has a major effect on particle size as well as the percentage of drug entrapment efficiency. Changing the concentration of surfactant from 1% to 2% may affect the particle size and entrapment efficiency of HG nanoparticles. When the surfactant concentration was raised from 1% to 2%, the particle size decreased, and drug entrapment increased. However, when the concentration was increased from 1% to 2%, the size of nanoparticles (nm) grew owing to particle aggregation, and the percent drug entrapped was found to be lowered (Table 1-3). HG nanoparticles and GG nanoparticles had PDI indexes of 0.062±0.04 and 0.068±0.09, respectively. HG and GG zeta potentials were found to be -12.9 mV and -6.12 mV, respectively (Table 3). The carboxyl moiety of the polymer, as well as the ligand, may be responsible for the negative zeta potential measurement of nanoparticles. Due to the greater repulsive contact, charged particles with a high zeta potential form more stable particles. The reduced negative zeta potential was shown to enhance the stability of the nanoparticle system.

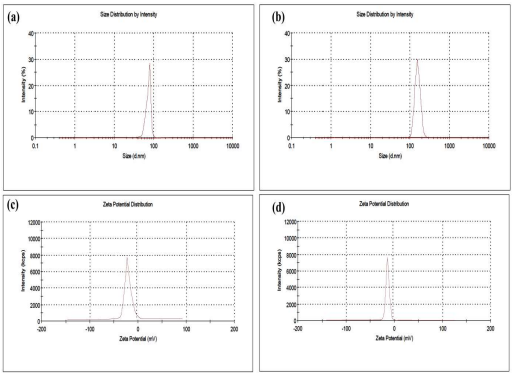

Fig. 4. Particle size of (a) HG NPs;(b) GG NPs and Zeta potential of (c) HGNPs; (d) GG NPs.

Differential scanning calorimetry (DSC) analysis

Differential Scanning Calorimetry (DSC) thermograms were obtained for HA, ADH, GG, 5-FU, HG NPs, and 5-FU-loaded HG NPs (Fig. 5), revealing distinct endothermic peaks at specific temperatures for each component.

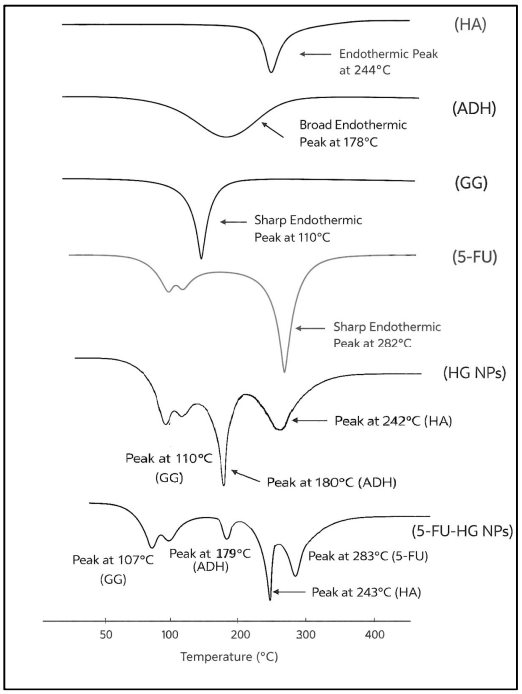

Fig. 5. DSC thermogram: (a) FA;(b) 5-FU; (c) FG (without 5-FU); (d) FG (with 5-FU).

Hyaluronic Acid (HA) exhibited an endothermic peak at 244°C, attributed to its polysaccharide structure, consistent with its typical thermal behavior. Adipic Acid Dihydrazide (ADH) exhibited a broad endothermic peak at 178°C, indicating dehydration and melting of its hydrazide groups, characteristic of its polymeric structure. For Gellan Gum (GG), a sharp endothermic peak at 110°C suggested the melting or glass transition of its polymer, indicating its typical thermal degradation. In HG Nanoparticles (HG NPs), without the drug, distinct peaks at 242°C, 180°C, and 110°C were observed for HA, ADH, and GG, respectively, confirming the presence of these components in the nanoparticle formulation. For 5-FU-loaded HG Nanoparticles (5-FU-HG NPs), an endothermic peak at 283°C was observed, corresponding to the crystalline form of 5-FU within the nanoparticle structure, with additional peaks for HA, ADH, and GG at 243°C, 179°C, and 107°C, respectively, indicating minimal alteration by the drug incorporation. The presence of an exothermic peak at 283°C in the thermogram of 5-FU-loaded HG NPs suggests that 5-FU remains encapsulated in a crystalline state, which may influence its release profile and bioavailability in pharmaceutical applications.

In-vitro drug release pattern

The graph shown in Figure 6 illustrates the sustained and extended release profile of 5-Fluorouracil (5-FU) from a nanoparticle system. The graph provides a detailed representation of the controlled and long-term release behavior of 5-FU

from both HG nanoparticles and plain polymeric Gellan Gum (GG) nanoparticulate systems. In the case of plain GG nanoparticles, 91.21% of 5-FU was released within 12 hours, indicating a relatively rapid release compared to the HG nanoparticles. However, HG nanoparticles exhibited a much slower, extended release of 5-FU, with 97.87% of the drug released over 48 hours. This prolonged release can be attributed to the formation of crosslinked core-shell micelles within HG nanoparticles, which provide a more controlled release mechanism.

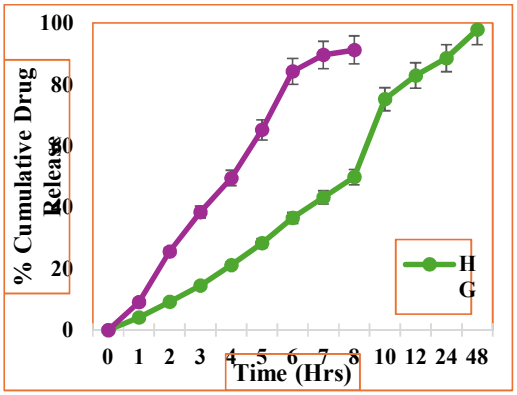

Fig.6. Percentage cumulative 5-FU release of FG and GG NPs

The slower release rate of 5-FU from the HG nanoparticle system is likely due to the solvent system used in nanoparticle preparation. Acetone and isopropyl alcohol, the solvents employed in the manufacturing process, are believed to break the hydrogen bonds present in Hyaluronic Acid (HA). This disruption promotes the reaction between the carboxyl group of HA and the amine group of Adipic Acid Dihydrazide (ADH) via carbodiimide conjugation, leading to the formation of a crosslinked structure. The crosslinking of the core-shell micelles reduces the overall solubility of the nanoparticles, resulting in a slower drug-release rate compared to plain GG nanoparticles, which do not undergo such extensive crosslinking. Thus, the HG nanoparticle system not only offers extended drug release over a longer duration but also demonstrates a more effective encapsulation of 5-FU, which could potentially improve the therapeutic outcomes in drug delivery systems by providing controlled, sustained release over an extended period.

Hemolytic toxicity study

A hemolytic toxicity study was conducted to assess the hemotoxic impact of the designed HA-anchored Gellan Gum (GG) nanoparticles (HG NPs) and plain GG nanoparticles. The research evaluated the hemolytic toxicity of plain 5-FU, 5-FU-loaded HG NPs, and 5-FU-loaded GG NPs by measuring the percentage hemolysis in distilled water. The results indicated that plain 5-FU exhibited hemolytic toxicity of up to 22.63%, while 5-FU-loaded HG NPs and 5-FU-loaded GG NPs showed lower hemolytic toxicity levels of 4.27% and 9.70%, respectively.

Among the 5-FU-loaded formulations, 5-FU-loaded HG NPs exhibited lower hemotoxicity compared to 5-FU-loaded GG NPs. This reduced toxicity could be attributed to the hydrophilic nature of Hyaluronic Acid (HA), which contributes to the hemocompatibility of the HG nanoparticle system. HA, being a naturally occurring biopolymer, is known for its biocompatibility and minimal toxicity in the bloodstream. The hydrophilic character of HA likely enhances the interaction with blood components in a non-toxic manner, ensuring the nanoparticle system's compatibility with human blood. The findings from this study align with similar research on nanoparticle systems in the literature, particularly a study by Garg et al. (2016), which highlighted that the suppression of drug-induced hemotoxicity in nanoparticle formulations may be related to factors such as nanoparticle surface chemistry and drug-release characteristics. The reduced hemotoxicity observed in 5-FU-loaded HG NPs supports the notion that incorporating hydrophilic biopolymers, such as HA, into nanoparticle systems may be a promising strategy for reducing hemotoxic effects while maintaining drug efficacy. This suggests that HA-anchored nanoparticles could be a safer and more effective option for drug delivery in clinical applications.

SRB (sulforhodamine B) assay

The SRB (Sulforhodamine B) assay was employed for in-vitro cytotoxicity screening of nanoparticles in the A549 human lung cancer cell line. This assay effectively measures the cell growth inhibition and viability of cells treated with varying concentrations of nanoparticle formulations. The results from the assay confirm a dose-dependent evaluation of cytotoxicity, where the cellular bioavailability of the nanoparticles significantly decreases as the concentration of the sample increases. HG nanoparticles loaded with 5-FU (5-Fluorouracil) were tested for their cytotoxic effects, and the results clearly show the consequences of these nanoparticles on cell growth inhibition. As shown in Figure 7, higher concentrations of 5-FU significantly limit cell proliferation, indicating that the presence of 5-FU, whether in its free or nanoparticle-encapsulated form, impairs the cell's ability to proliferate. Furthermore, as the 5-FU concentration increases, cell viability decreases markedly, underscoring the drug's cytotoxicity. Both free 5-FU and 5-FU-loaded nanoparticles (including HG NPs and GG NPs) were evaluated.

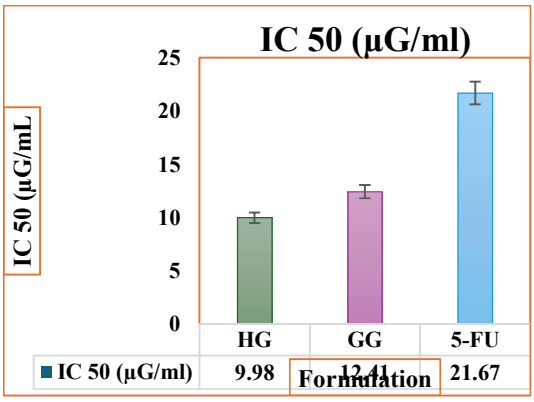

Fig. 7(a). *IC50* of 5-FU, HG NPs and GG NPs in A549 Cancer cellline

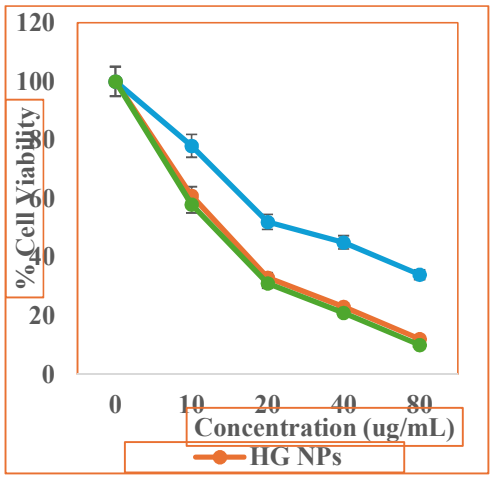

Fig. 7(b). *In-vitro* percentage control growth of 5-FU, HG NPs and GG NPs in A549 Cancer cellline

The nanoparticles, when compared to free 5-FU, exhibited higher cytotoxicity at concentrations between 10-80 µg/mL. This suggests that the nanoparticle formulations are more effective in delivering 5-FU, enhancing its therapeutic efficacy.

The percentage growth inhibition data from the A549 cells showed a clear inverse relationship between 5-FU concentration and cell growth, with higher 5-FU concentrations leading to greater inhibition of cellular proliferation. Notably, compared with free 5-FU, the nanoparticle formulations (both HG NPs and GG NPs) exhibited significantly higher cytotoxicity across the 10-80 µg/mL concentration range.

To quantify the cytotoxicity, the IC50 values (the concentration of drug required to inhibit 50% of cell viability) were calculated using the linear regression equation Y = Mx + C. The IC50 values for 5-FU, GG NPs, and HG NPs were calculated as 21.67 µg/mL, 12.41 µg/mL, and 9.98 µg/mL, respectively. These results clearly show that 5-FU-loaded HG NPs exhibit the lowest IC50 value, indicating they are the most effective at reducing cell viability among the formulations. This highlights the potential of HG NPs as an efficient drug delivery system, offering enhanced cytotoxicity and therapeutic efficacy in cancer treatment.

mTOR assay

The statistical data from the mTOR expression study by flow cytometry provides valuable insights into the effects of HG NPs and GG NPs on mTOR expression in A549 cells. According to the observations, untreated A549 cells exhibited high mTOR expression, with a mean fluorescence intensity (MFU) of 71.87. In contrast, the test compound (HG NPs) demonstrated a significant reduction in mTOR expression, with an IC50 concentration of 9.98 µg/mL, showing a mean fluorescence intensity (MFU) of 16.43. This notable reduction in mTOR expression suggests that HG NPs effectively suppress or downregulate mTOR, pointing to their potential as a therapeutic targeting the mTOR signaling pathway, which is commonly implicated in cancer cell growth and proliferation. Further comparison with GG NPs revealed a mean fluorescence intensity of 28.98 at an IC50 concentration of 12.41 µg/mL. This also represented a significant decrease in mTOR expression compared to the control group (71.87 MFU), although not as pronounced as the effect observed with HG NPs. The GG NPs also demonstrated downregulation of mTOR, indicating that both formulations, HG NPs and GG NPs, can influence mTOR signaling, but HG NPs appear to be more potent in this regard.

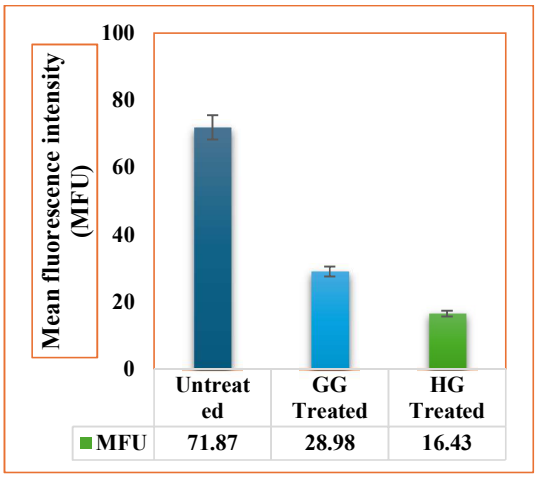

Figure 8. The mean fluorescence intensity of mTOR-FITC against the Untreated and drug treated A549 cells and overlay of the results plotted in Bar graph.

The findings strongly suggest that both HG NPs and GG NPs suppress mTOR expression, with HG NPs exhibiting the most pronounced inhibition. Given that mTOR is a critical component of the

PI3K/Akt/mTOR signaling pathway, which is involved in cell growth, survival, and metabolism, the results of this study provide compelling evidence that HG NPs and GG NPs have therapeutic potential in treating diseases associated with lung cancer and other mTOR-driven disorders. By downregulating mTOR expression, these nanoparticles could potentially reduce cancer cell proliferation and enhance therapeutic outcomes in lung cancer treatment. The observed reduction in mTOR expression also suggests that these nanoparticle formulations may play a critical role in targeted drug delivery systems, thereby improving drug efficacy and minimizing side effects associated with conventional therapies.

p53 expression

The statistical data from the p53 expression study by flow cytometry provides significant insights into the p53 expression levels in A549 cells upon treatment with HG NPs and GG NPs. The results reveal that untreated A549 cells exhibit very low expression of p53, with a mean fluorescence intensity (MFU) of 6.43, indicating that p53 levels are generally suppressed or inactive in these cells, which is characteristic of many cancerous cells that evade apoptosis. However, when treated with HG NPs, a remarkable increase in p53 expression was observed. Specifically, at the IC50 concentration of 9.98 µg/mL, the HG NPs treatment resulted in a mean fluorescence intensity (MFU) of 61.28, demonstrating a substantial upregulation of p53 expression.

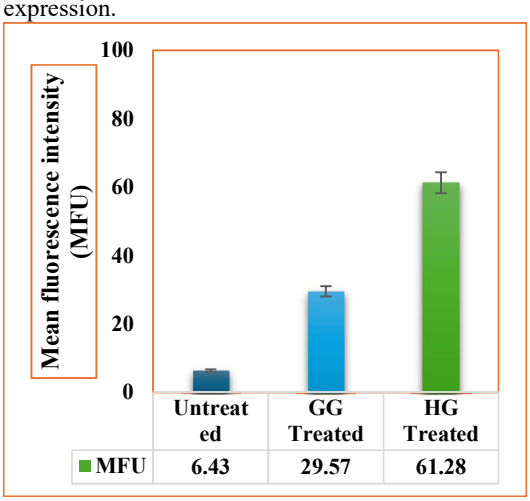

Figure 9. The mean fluorescence intensity of p53-FITC against the Untreated and drug-treated A549 cells

This upregulation suggests that HG NPs may effectively restore p53 function, a crucial tumor suppressor gene known for its role in inducing apoptosis and regulating the cell cycle in response to DNA damage. The observed increase in p53 expression indicates that HG NPs may have a therapeutic potential in lung cancer and other cancers where p53 mutations or inactivation are common.

On the other hand, GG NPs also increased p53 expression, but to a lesser extent. GG NPs showed a mean fluorescence intensity of 29.57 at an IC50 concentration of 28.98 µg/mL, indicating some level of p53 upregulation compared to the untreated A549 cells, but still much lower than the effect seen with HG NPs. The p53 expression in the control cells remained at 6.43 MFU, confirming that the nanoparticles were responsible for the observed changes in expression levels.

These observations strongly suggest that the HG NPs have the potential to enhance p53 expression, thereby restoring apoptotic pathways and inhibiting cancer cell survival in lung cancer cells. The upregulation of p53 by HG NPs suggests a possible role in reversing the dysfunction of tumor suppressor genes, which is often a critical step in cancer therapy. In comparison, while GG NPs also showed some p53 activation, HG NPs appear to have a more potent effect, suggesting they may offer a more effective therapeutic approach for lung cancer-derived diseases. This further supports the hypothesis that HG NPs can serve as a promising drug delivery system, capable of targeting and modulating tumor suppressor pathways to achieve therapeutic benefits. Thus, the p53 expression findings provide essential justification for continued exploration of HG NPs in cancer treatment, particularly in therapies targeting lung cancer.

Apoptosis Assay

The results of the Annexin-V/PI staining assay on A549 lung cancer cells after treatment with 5-FU, HG NPs, and GG NPs for 24 hours reveal important insights into the cytotoxic effects and apoptosis induction of these formulations (Fig 7.10).

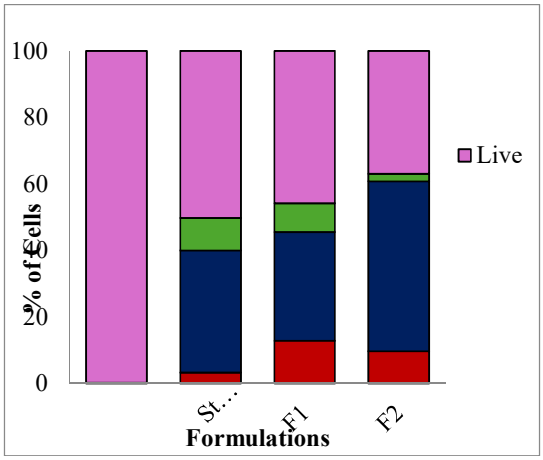

Figure 10. Quadrant plots representing the % of population of live, apoptosis and necrotic A549 cells treated with 5FU, HG NPs (F1), and GG NPs (F2).

The untreated A549 cells displayed 99.9% live cells, with only 0.1% early apoptosis, indicating that the cells were largely viable and showed minimal signs of stress or apoptosis. However, when treated with 5-FU, there was a noticeable increase in late apoptosis (33.32%) and early apoptosis (12.17%), with 50.67% of the cells remaining viable. These findings suggest that while 5-FU effectively induces apoptosis in a significant portion of the cells, it does not completely eliminate cell viability, indicating the potential for 5-FU resistance or insufficient drug action in some cells.

The treatment with HG NPs, however, demonstrated a marked improvement in apoptosis induction, with 37.57% of cells undergoing late apoptosis and 7.91% early apoptosis, resulting in 45.75% viable cells. These results suggest that HG NPs are more effective at inducing apoptosis than free 5-FU, likely due to the nanoparticle formulation's ability to enhance drug delivery, improve drug uptake by cells, and provide controlled, sustained release of 5-FU, thereby overcoming some of the limitations observed with free drug administration. On the other hand, GG NPs also induced apoptosis, though to a lesser extent than HG NPs, with 35.43% of cells undergoing late apoptosis, 6.27% in early apoptosis, and 49.51% remaining viable. While GG NPs exhibited some cytotoxic effects, their overall efficacy in inducing apoptosis was less pronounced than that of HG NPs, suggesting that the hydrophilic nature of HA in HG NPs may play a significant role in improving therapeutic response. The comparative analysis of HG NPs, GG NPs, and free 5-FU underscores the superior potential of HG NPs to induce apoptosis in A549 lung cancer cells, which could significantly enhance drug efficacy and reduce side effects associated with traditional chemotherapy. The findings suggest that 5-FU-loaded HG NPs have considerable potential as a drug delivery system for lung cancer therapy, offering a more effective therapeutic strategy by modulating cellular apoptosis and improving cancer treatment outcomes.

Conclusion

The characterization studies confirmed the successful synthesis and superior performance of hyaluronic acid–adipic acid dihydrazide–gellan gum (HG) nanoparticles. FTIR and ^{1}H-NMR analyses verified the successful conjugation of HA, ADH, and GG through the formation of stable amide linkages. AFM images demonstrated that HG nanoparticles possessed a uniform spherical morphology with particle sizes ranging from 81–206 nm, whereas GG nanoparticles exhibited comparatively larger particle size and slight aggregation. The zeta potential of HG nanoparticles (−12.9 mV) indicated better colloidal stability than GG nanoparticles (−6.12 mV). DSC thermograms confirmed the successful encapsulation of 5-fluorouracil (5-FU) without significant alteration of the polymeric matrix. The HG nanoparticles exhibited a high drug release of 97.87% over 48 h, demonstrating sustained and controlled release compared with GG nanoparticles (91.21% within 12 h). Hemolytic studies revealed excellent hemocompatibility, with HG nanoparticles producing only 4.27% hemolysis, significantly lower than GG nanoparticles (9.70%) and free 5-FU (22.63%). The SRB assay showed enhanced cytotoxicity of HG nanoparticles against A549 lung cancer cells, with an IC_{50} of 9.98 µg/mL, compared with GG nanoparticles (12.41 µg/mL) and free 5-FU (21.67 µg/mL). Furthermore, flow cytometric analysis demonstrated significant mTOR inhibition, upregulation of p53 expression, and increased Annexin V/PI-mediated apoptosis in HG nanoparticle-treated cells. Overall, these findings indicate that 5-FU-loaded HG nanoparticles provide superior stability, controlled drug release, enhanced biocompatibility, targeted anticancer activity, and effective modulation of the PI3K/AKT/mTOR signaling pathway, highlighting their potential as an advanced nanocarrier for targeted lung cancer therapy.

References

Bhadra, D., Yadav, A. K., Bhadra, S., & Jain, N. K. (2005). Glycodendrimeric nanoparticulate carriers of primaquine phosphate for liver targeting. *International journal of pharmaceutics*, *295*(1-2), 221–233. https://doi.org/10.1016/j.ijpharm.2005.01.026

Deng, Z., Qing, Q., & Huang, B. (2024). A bibliometric analysis of the application of the PI3K-AKT-mTOR signaling pathway in cancer. Naunyn-Schmiedeberg's archives of pharmacology, 397(10), 7255–7272. https://doi.org/10.1007/s00210-024-03112-9

Fruman, D. A., Chiu, H., Hopkins, B. D., Bagrodia, S., Cantley, L. C., & Abraham, R. T. (2017). The PI3K pathway in human disease. *Cell, 170*(4), 605–635. https://doi.org/10.1016/j.cell.2017.07.029

Garg, A., Rai, G., Lodhi, S., Jain, A. P., & Yadav, A. K. (2016a). In-vitro and in-vivo assessment of dextran-appended cellulose acetate phthalate nanoparticles for transdermal delivery of 5-fluorouracil. Drug Delivery, 23(5), 1525–1535. https://doi.org/10.3109/10717544.2014.978512

Garg, A., Garg, S., Sahu, N. K., Rani, S., Gupta, U., & Yadav, A. K. (2019). Heparin appended ADH-anionic polysaccharide nanoparticles for site-specific delivery of usnic acid. *International journal of pharmaceutics*, *557*, 238–253. https://doi.org/10.1016/j.ijpharm.2018.12.049

Garg, A., Rai, G., Lodhi, S., Jain, A. P., & Yadav, A. K. (2016b). Hyaluronic acid embedded cellulose

acetate phthlate core/shell nanoparticulate carrier of 5-fluorouracil. *International journal of biological macromolecules*, *87*, 449–459. https://doi.org/10.1016/j.ijbiomac.2015.11.094

Huang, G., & Huang, H. (2018). Hyaluronic acid-based biopharmaceutical delivery and tumor-targeted drug delivery system. *Journal of Controlled Release, 278*, 122–126. https://doi.org/10.1016/j.jconrel.2018.03.021

Janku, F., Yap, T. A., & Meric-Bernstam, F. (2018). Targeting the PI3K pathway in cancer: Are we making headway? *Nature Reviews Clinical Oncology, 15*(5), 273–291. https://doi.org/10.1038/nrclinonc.2018.28

Liu, Y., Zhang, X., & Wang, J. (2022). Polysaccharide-based nanoparticles for targeted cancer therapy: Recent advances and future perspectives. *Carbohydrate Polymers, 287*, 119332.

Misra, S., Heldin, P., Hascall, V. C., Karamanos, N. K., Skandalis, S. S., Markwald, R. R., & Ghatak, S. (2015). Hyaluronan-CD44 interactions as potential targets for cancer therapy. *FEBS Journal, 282*(18), 3525–3540.

Mitragotri, S., Lammers, T., Bae, Y. H., Schwendeman, S., De Smedt, S., Leroux, J. C., et al. (2021). Drug delivery research for the future. *Nature Reviews Drug Discovery, 20*(1), 1–2.

Osmałek, T., Froelich, A., & Tasarek, S. (2014). Application of gellan gum in pharmacy and medicine. *International Journal of Pharmaceutics, 466*(1–2), 328–340.

Pang, X., Liu, H., Long, Y., & Wang, H. (2026). mTOR in radiotherapy of lung cancer: Mechanisms of radiation resistance and therapeutic implications (Review). *International journal of oncology*, *68*(2), 21. https://doi.org/10.3892/ijo.2025.5834

Qiang, M., Chen, Z., Liu, H., Dong, J., Gong, K., Zhang, X., Huo, P., Zhu, J., Shao, Y., Ma, J., Zhang, B., Liu, W., & Tang, M. (2025). Targeting the PI3K/AKT/mTOR pathway in lung cancer: mechanisms and therapeutic targeting. *Frontiers in pharmacology*, *16*, 1516583. https://doi.org/10.3389/fphar.2025.1516583

Shi, J., Kantoff, P. W., Wooster, R., & Farokhzad, O. C. (2020). Cancer nanomedicine: Progress, challenges and opportunities. *Nature Reviews Cancer, 20*(2), 73–92.

Volpi, N., Schiller, J., Stern, R., & Soltés, L. (2021). Role, metabolism, chemical modifications and applications of glycosaminoglycans. *Current Medicinal Chemistry, 28*(5), 903–927.

Weng, J., Tong, H. H. Y., & Chow, S. F. (2020). In Vitro Release Study of the Polymeric Drug Nanoparticles: Development and Validation of a Novel Method. *Pharmaceutics*, *12*(8), 732. https://doi.org/10.3390/pharmaceutics12080732

Zhang, Y., Li, X., Wang, H., & Chen, J. (2023). Hyaluronic acid-functionalized nanoparticles for targeted cancer therapy: Advances and prospects. *International Journal of Biological Macromolecules, 242*, 124885.